

# Detectability of Lensed Continuous Gravitational Waves from Galactic Neutron Stars

## Abstract.

This paper delves into the nature and observability of continuous gravitational waves being lensed by massive objects, such as the supermassive black hole located at the center of our galaxy (Sagittarius A\*). In the first part, we look at the theoretical framework developed through several decades, specifically, we will use the Nakamura and Takashi [1] formalism to quantitatively express the amplification of a gravitational wave as it travels through the compact lens. The second part will look at how the diffraction pattern arises and how we can observe this modulation as we traverse the plane. In the third part we assess the expected source population in the galactic bulge and quantitatively estimate the number of pulsars we believe to be lensed spanning the galactic bulge. By integrating over various density functions for neutron star populations, the number of sources we would expect to be lensed is approximately  $15 \pm 3$ . This last value was then used in the final part where a Monte Carlo simulation for the maximum amplification factor is carried out. We considered a Poisson distribution with  $\lambda = 15$  to draw the number of sources during the Monte Carlo simulation. By selecting only the maximally amplified sources, results show how the amplification factor is weakly dependent of frequency, therefore suggesting that gravitational waves with any radiation frequency will be equally amplified. The simulation also showed the most probable amplification factor to be  $F = 1.85$ .

## 1. Introduction

Ever since Einstein's first publication of General Relativity (GR) [2], scientists have been able to describe many astrophysical phenomena occurring in our universe, whereas a classical (Newtonian) description could not. One of the many successful predictions of GR was the existence of gravitational microlensing. This occurs when a light ray, traveling along a null geodesic, alters its direction of motion in the vicinity of massive bodies.[1, 3, 4] This distortion causes the light from distant galaxies or stars to bend as observed from Earth. Thousands of lensing phenomena have been observed throughout the last century, and with the recent successful detections of Gravitational Waves (GW), by the LIGO and VIRGO teams [5], and with the future upgrades(aLIGO, AdVIRGO) and new detectors, such as the Einstein Telescope and Cosmic Explorer, and space bound interferometers, such as the Laser Interferometer Space Antenna (LISA), the number of such observable events will drastically increase in the upcoming years. In the weak field approximation, the wave optics description of lensed waveforms applies not only to electromagnetic radiation, but also to GWs. This has lead to the conclusion that continuous gravitational wave sources, such as fast rotating neutron stars (NSs) and binary white dwarfs (WD-WD), would be the best probing mechanism to detect this lensing phenomena, due to their long-lived gravitational radiation. Furthermore, the lensing event will produce amplification fringes of the GW. These fringes not only will amplify the GW signal, but will further confirm the wave nature of these space-time perturbations [3].

The display of the lensing effects depend principally on two main factors: the lens mass scale,

$M$ , and the wavelength of the radiation,  $\lambda$ . If the wavelength is much longer than the lens mass scale <sup>1</sup>,  $M \ll \lambda$ , then the wave optics limit describes the lensing appropriately, otherwise, the wave behaves according to the geometric optics limit, described by Fermat's principle [1, 4]. In this report we will concentrate on the latter, where gravitational waves are being emitted by rotating neutron stars lensed by the super massive black hole at the center of the Milky Way (Sagittarius A\*), with  $M = 2 \times 10^6 M_\odot$  ( $\approx 4 * 10^9$  m) [6] and radiation wavelength of the order of  $\lambda \approx 10^6$  m [7]. After having analyzed the wave effects of GWs being lensed by Sag A\*, the last section will delve into computing a Monte Carlo simulation of the amplification factor varying both source position and frequency, thus giving a measure of feasibility on whether we can detect these effects using third generation detectors. In the following sections, we have assumed  $G = c = 1$ .

## 2. Theoretical Framework

### 2.1. Wave Optics of Gravitational lensing

Consider a space-time metric background, perturbed linearly, as follows:

$$g_{\mu\nu} = g_{\mu\nu}^{(B)} + h_{\mu\nu} \quad (1)$$

where  $g_{\mu\nu}^{(B)}$  is the background, unperturbed, metric, and  $h_{\mu\nu}$  is the linear perturbation caused by the GW [1]. As the waves propagate through a weak gravitational potential of the lens, the spacetime background metric would be defined as [8]:

$$ds^2 = -(1 + 2U(r, \theta, \phi))dt^2 + (1 - 2U(r, \theta, \phi))(dr^2 + r^2d\theta^2 + r^2 \sin^2(\theta)d\phi^2) = g_{\mu\nu}^{(B)}dx^\mu dx^\nu \quad (2)$$

Where  $U(r, \theta, \phi)$  is the Newtonian gravitational potential described by the lens and  $\mathbf{r} = (r, \theta, \phi)$  are spherical coordinates. The GW will interact only in a small region located around the lens, compared to the large distances considered between source and observer. Then, under the traceless-transverse Lorentz Gauge condition, it follows [1]:

$$h_{\mu\nu;\alpha}{}^{\dot{\alpha}} + 2R_{\alpha\mu\beta\nu}^{(B)}h^{\alpha\beta} = 0 \quad (3)$$

where  $R_{\alpha\mu\beta\nu}^{(B)}$  is the background Riemann Tensor. Assuming the wavelength,  $\lambda$  is much smaller than the typical radius of curvature, we can set  $h_{\mu\nu;\alpha}{}^{\dot{\alpha}} = 0$ , since the curvature component would be close to zero. We can further approximate this by considering the eikonal approximation, in which we express the GW as  $h_{\mu\nu} = \Phi e_{\mu\nu}$ , where  $\Phi$  is the scalar field and  $e_{\mu\nu}$  is the polarization tensor. Since the gravitational lensing is of the order ( $U \ll 1$ ), we can assume that the change of the polarization tensor is practically zero, thus rendering it a constant as the GW gets lensed [1]. Therefore, the scalar field,  $\Phi$ , will propagate following the Klein-Gordon equation for curved spacetimes, as follows [1, 9]:

$$\square\Phi(\vec{r}, t) = \frac{\partial}{\partial x^\mu} \left( \sqrt{-g^{(B)}} g^{(B)\mu\nu} \frac{\partial}{\partial x^\nu} \right) \Phi(\vec{r}, t) \quad (4)$$

where  $g^{(B)} = g_{\mu\nu}g^{\mu\nu}$ . The GW can be considered as a monochromatic wave incoming from a point source. Hence, we can describe the complex amplitude as follows:

$$\Phi(\mathbf{r}, t) = \frac{A}{|\mathbf{r}|} F(\mathbf{r}) e^{-i(\omega t - \mathbf{k} \cdot \mathbf{r})} \quad (5)$$

<sup>1</sup> Note: The lens mass scale is in units of distance, since it was multiplied by the factor  $\frac{G}{c^2}$

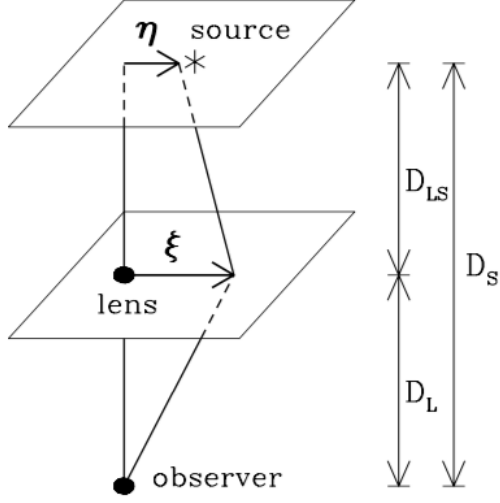


**Figure 1:** Setup diagram of observer-lens-source with noted distances of  $D_S$ ,  $D_L$  and  $D_{LS} = D_S - D_L$ , which are respectively source-observer, lens-observer and source-lens distances. The source offset,  $\eta$ , and the path distance from the lens,  $\xi$ , have been both parameterized in units of impact parameter,  $\xi_0 = \theta_E D_L$ , where  $\theta_E$  is the Einstein angle. Source of image [1].

Where  $A$  is a constant,  $F(\mathbf{r})$  is the amplification factor,  $\omega = 2\pi f$  is the angular natural frequency of the wave,  $f$  is the GW frequency and  $\mathbf{k}$  is the wave number vector. Therefore, inserting Eq.(2) and Eq.(5) into Eq.(4), the propagation equation follows [10]:

$$\frac{\partial^2 F}{\partial r^2} + 2i\omega \frac{\partial F}{\partial r} + \frac{1}{r^2 \sin \theta} \left[ \frac{\partial}{\partial \theta} \left( \sin \theta \frac{\partial F}{\partial \theta} \right) + \frac{1}{\sin \theta} \frac{\partial^2 F}{\partial \phi^2} \right] - 4\omega^2 U(\vec{r})F = 0 \quad (6)$$

To solve Eq.(6) the Kirchhoff Integral is used [11]. Due to [1] formalism, it is appropriate to write the amplification factor as:

$$F = \frac{\tilde{\Phi}^L}{\tilde{\Phi}} \quad (7)$$

where the tilde defines frequency domain(i.e.  $\tilde{\Phi}(f, \mathbf{r})$ ), and the numerator and denominator are the lensed and unlensed wave forms respectively (i.e. unlensed  $U = 0$ ). Then, assuming the rate of change of the amplification factor in the radial direction (i.e. the second term,  $2i\omega \frac{\partial F}{\partial r}$ ) is on the same scale of the ratio of the amplification factor over the wavelength, the first term can be neglected compared to the second one (eikonal approximation) [8, 10]. Under this assumption, Eq.(6) resembles the Schrödinger equation, where  $\omega$ ,  $t$  and  $2\omega U(r, \theta)$  are the particle mass, “time” component in  $r$  and the “time dependent potential” respectively [8].

Two important parameters that allow us to describe the lensing phenomena are the Einstein angle and the dimensionless frequency parameter, defined as:

$$\theta_E = \sqrt{4M \frac{D_{LS}}{D_S D_L}} \quad (8)$$

$$w = 8\pi M_{lz} f \quad (9)$$

where  $D_L$ ,  $D_S$ ,  $D_{LS}$  are the distances observer-lens, observer-source, lens-source respectively , shown in Fig.1. The parameter  $M_{lz} = (1+z_l)M$  is the redshift mass<sup>2</sup> of the lens and  $f$  is the GW frequency [1]. It is clear the  $w$  in Eq.(9) is proportional to  $M/\lambda$ , therefore the quantity of this parameter tells us which types of optics more appropriately describes the lensing phenomena (wave or geometric). In the case for nearby galactic sources,  $z = 0$ , therefore  $M_{lz} = M$ . Assuming thin lens approximation , with lens mass distribution  $\Sigma(\xi)$ , where  $\xi$  is the impact parameter (radial position of path ray on the lens plane) and assuming GWs scatter on the thin lens plane [1], the solution to Eq.(6) at the observer is [10, 11, 12]:

$$F(w, y) = \frac{w}{2\pi i} \int e^{iwT(\mathbf{x}, \mathbf{y})} d^2 \mathbf{x} \quad (10)$$

where  $T(\mathbf{x}, \mathbf{y})$  is the time delay function, defined as follows:

$$T(\mathbf{x}, \mathbf{y}) = \frac{1}{2} |\mathbf{x} - \mathbf{y}|^2 - \psi(\mathbf{x}) + \phi_m(y) \quad (11)$$

where we have introduced the dimensionless quantities as:  $\mathbf{x} = \boldsymbol{\xi}/\xi_0$  ,  $\mathbf{y} = \boldsymbol{\eta}D_L/D_S\xi_0$  , which are the source offset and the path distance offset in units of Einstein radius,  $\xi_0 = \theta_E D_L$ , where  $\theta_E$  and  $D_L$  are the Einstein angle and lens distance respectively. The variables  $\boldsymbol{\eta}$  and  $\boldsymbol{\xi}$  are position vectors on the source and lens planes respectively. The time delay function in Eq.(11), as the name suggests, describes the time delay the GW acquires as it traverses the gravitational potential. In gravitational lensing, the lensing object will interact with the GW following the lens classical (no relativity) equation [11], described as follows:

$$\mathbf{x} + \mathbf{y} - \nabla\psi(\mathbf{x}) = 0 \quad (12)$$

where  $\psi(\mathbf{x}) = \int_{-\infty}^{\infty} dz U$  is the two dimensional gravitational potential. Solving Eq.(12) gives the positions of images of the source being lensed over the lens plane,  $\mathbf{x}$ . For a point mass lens,  $\psi(\mathbf{x}) = \ln(\mathbf{x})$ , the image positions would be  $\mathbf{x}_{\pm} = \mathbf{y}/2 + \sqrt{\mathbf{y}^2 + 4}/2$ . Therefore, the two formed images will have an arrival time difference due to the time delay function. For simplicity,  $\phi_m$  was inserted in Eq.(11) as an arbitrary function which allows setting the minimum delay time equal to zero [1]. Further generalization of Eq.(10) can be carried out by considering the case of a symmetric lens model. In this case, the gravitational potential  $\psi(\mathbf{x})$  will only depend on  $x = |\mathbf{x}|$ , allowing us to rewrite (10) as follows [1, 4, 12]:

$$F(w, y) = -iwe^{\frac{i}{2}wy^2} \int_0^{\infty} x J_0(wxy) e^{iw[\frac{1}{2}x^2 - \psi(x) + \phi_m(y)]} dx \quad (13)$$

where  $J_0(wxy)$  is the first order Bessel function and  $y = |\mathbf{y}|$ . From now on, we define  $x = |\mathbf{x}|$  and  $y = |\mathbf{y}|$

## 2.2. Point Mass lens and Singular Isothermal Sphere

In this section we consider two mass lens distributions, the *point mass* (PM) and the *singular isothermal sphere* (SIS). First let us recall the definition of the gravitational deflection potential,  $\psi(\mathbf{x})$ , and the surface mass density,  $\Sigma(\mathbf{x})$ , as follows:

$$\psi(\mathbf{x}) = 4 \frac{D_L D_{LS}}{D_S} \int_{-\infty}^{\infty} \Sigma(\mathbf{s}) \ln |\mathbf{x} - \mathbf{s}| d^2 \mathbf{s} \quad (14)$$

$$\Sigma(\mathbf{x}) = \int_{-\infty}^{\infty} \rho(\mathbf{x}, z) dz \quad (15)$$

<sup>2</sup> Note: The lens mass scale is in units of time, since it was multiplied by the factor  $\frac{G}{c^3}$

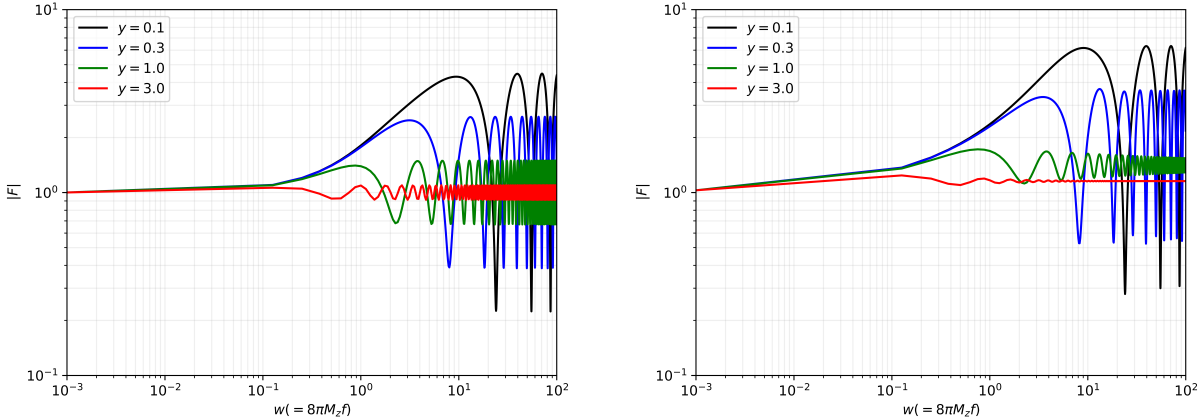


**Figure 2:** *Left:* Amplification factor for the point mass lens model for different fixed source positions ( $y$  is dimensionless). As the source position grows, the amplification gets highly damped. *Right:* Amplification factor for the SIS model. For  $y \geq 1$ , the amplification is highly damped.

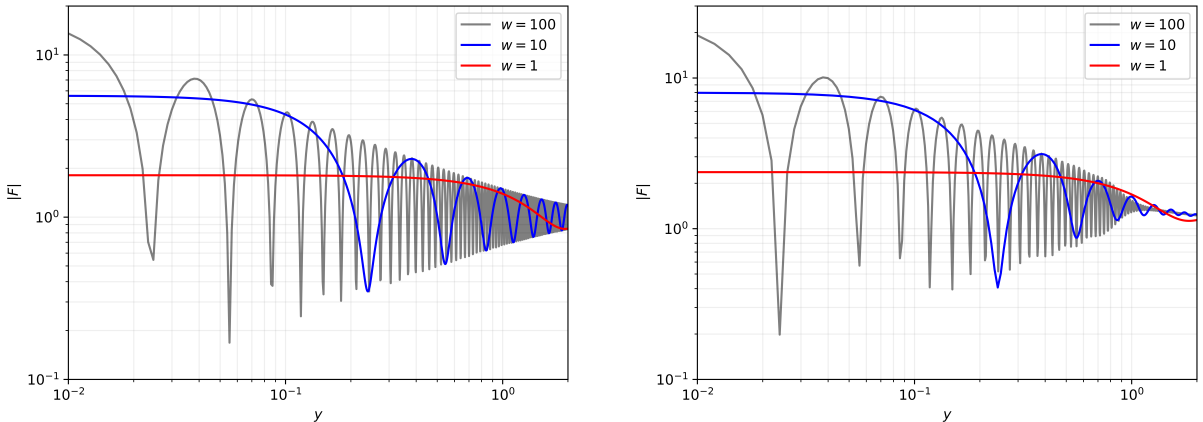


**Figure 3:** *Left:* Amplification factor for the point mass lens model for different fixed frequencies ( $y$  is dimensionless). *Right:* Amplification factor for the SIS model. For  $y \geq 1$ , the amplification is highly damped.

where  $\rho(\mathbf{x}, z)$  is the mass density distribution [12] over the lens plane. The surface mass density in the lens plane for the two cases are described in Table 1, where  $\delta(\xi)$  is the Delta function and  $\sigma_v$  is the dispersion velocity [1, 12, 4]. In the first model, the mass distribution describes point-like lenses, such as isolated stars. The SIS model is used for extended lenses, such as globular clusters. Inserting the equations for the deflection potential in Eq.(10), the amplification factor of the two models can be described analytically as follows (the solution to the equations are described in [13]):

$$F(w, y)_{\text{PM}} = e^{\frac{\pi w}{4} + i\frac{w}{2}(\ln(\frac{w}{2}) - 2\phi_m(y))} \Gamma\left(1 - \frac{i}{2}w\right) {}_1F_1\left(\frac{i}{2}w, 1; \frac{i}{2}wy^2\right) \quad (16)$$

$$F(w, y)_{\text{SIS}} = e^{\frac{i}{2}w(y^2 + 2\phi_m(y))} \sum_{n=0}^{\infty} \frac{\Gamma\left(1 + \frac{n}{2}\right)}{n!} \left(2we^{i3\pi/2}\right)^{n/2} {}_1F_1\left(1 + \frac{n}{2}, 1; -\frac{i}{2}wy^2\right) \quad (17)$$

**Table 1:** Table showing the lensing parameters for the point mass and SIS models.

Model	$\Sigma(\xi)$	$\theta_E$	$\psi(x)$	$w$
Point Mass	$M\delta(\xi)$	$\sqrt{4M \frac{D_{LS}}{D_S D_L}}$	$\ln x$	$8\pi M f$
Singular Isothermal Sphere	$\frac{\sigma_v^2}{2\xi}$	$4\pi\sigma_v^2 \frac{D_{LS}}{D_S}$	$x$	$2\pi f(4\pi\sigma_v^2)^2 \frac{D_L D_{LS}}{D_S}$

where Eq.(16) and Eq.(17) are the analytical solutions for the amplification factors for the PM and SIS lens models respectively. In Eq.(16),  $\phi_m(y) = (x_m - y)^2/2$ , where  $x_m$  is the positive image position computed from Eq.(12) [1]. In Eq.(17),  $\phi_m(y) = y + 1/2$  [12],  $\Gamma$  is the Gamma function and  ${}_1F_1$  is the confluent hyper geometrical function [14]. It is important to note the amplification factor for both models only includes two parameters, dimensionless frequency and source position (for fixed lens mass). Figure 2 shows the amplification factor for the point mass lens (left) and the SIS (right) model as a function of  $w$ . The oscillatory behavior is clearly visible as the frequency increases. Figure 3 shows the amplification factor as a function of source position for both lens model. As  $y$  tends to zero (source perfectly aligned with lens), the amplification factor converges. The value of the amplification factor at  $y = 0$  is:

$$|F(w, 0)_{PM}| = \sqrt{\frac{\pi w}{1 - e^{-\pi w}}} \quad (18)$$

$$\begin{aligned} |F(w, 0)_{SIS}| &= \left| \sum_{n=0}^{\infty} \frac{\Gamma\left(1 + \frac{n}{2}\right)}{n!} \left(2w e^{i3\pi/2}\right)^{n/2} \right| = \\ &= \left| 1 + \frac{1}{2}(1-i)e^{-\frac{1}{2}w} \sqrt{\pi w} \left[ 1 + \text{Erf}\left(\frac{\sqrt{w}}{2}(1-i)\right) \right] \right| \end{aligned} \quad (19)$$

See Appendix A for the derivation of the equation (18) and Appendix B for the derivation of (17) and (19).

### 2.3. Geometrical Optics

Taking the lens scale mass to be constant, the dimensionless frequency parameter increases as a function of frequency. If the frequency is high enough, ( $w \gg 1$ ), then the amplification factor can be reduced to the conventional geometrical limit approximation (usually used for EM radiation, where  $M \gg \lambda$ ). In this limit, Eq.(10) is computed around the stationary points (greatest contributions over the integral, due to the high oscillatory behavior of the function in the high frequency domain). The stationary points are evaluated by differentiating the time delay function with respect to the image position ( $x$ ) and setting it to zero, as follows:

$$\nabla_x T(\mathbf{x}, \mathbf{y}) = \mathbf{x} - \mathbf{y} - \nabla_x \psi(\mathbf{x}) = 0 \quad (20)$$

The solution to  $\mathbf{x}$  corresponds to the image positions in the geometric optics limit, and the condition for minimum time delay is expressed as Fermat's principle of least action [10]. For a strong gravitational deflection potential, the images formed are multiple (classically only two images are formed). From this we can Taylor expand the time delay around the  $x_i$  image as follows:

$$T(\mathbf{x}) = T(\mathbf{x}_i) + \frac{1}{2} \sum_{ab} \bar{x}_a \bar{x}_b \partial_a \partial_b T(\mathbf{x}_i) + \frac{1}{6} \sum_{abc} \bar{x}_a \bar{x}_b \bar{x}_c \partial_a \partial_b \partial_c T(\mathbf{x}_i) + \dots \quad (21)$$

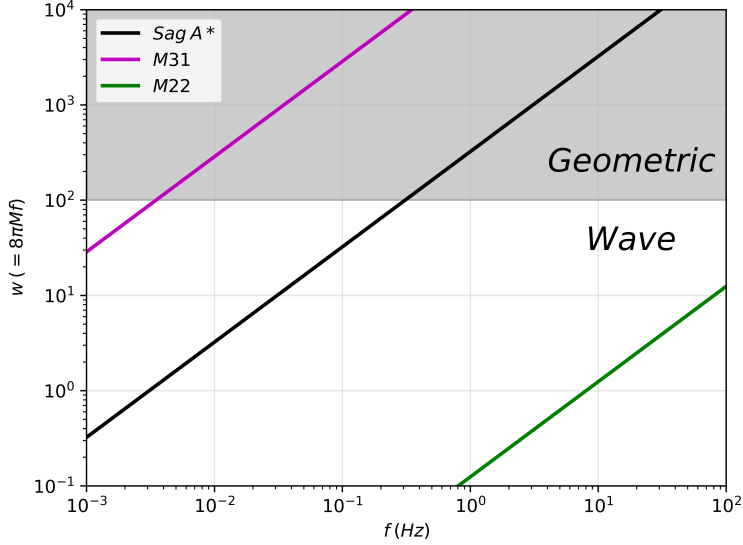


**Figure 4:** Dimensionless frequency parameter against radiation frequency. The different lines correspond to different lensing objects: “black” is Sagittarius A\*, “magenta” is the galactic center black hole of M31 (Andromeda galaxy) and the “green” line correspond to the globular cluster M22. The shaded grey area represents where the geometrical optic limit approximation is more appropriate when describing the lensing system ( $w \geq 100$  was set as a relative value for high radiation frequency)

where  $\bar{x} = x - x_i$  is the distance between the first and the  $i$ th image, as the indices  $abc$  run from 0 to 2, which correspond to the minimum, saddle and maximum points of the time delay function respectively. If the frequency gets large enough ( $w \gg 1$ ), then  $w|\partial^2 T|^3 \gg |\partial^3 T|^2$ ,  $w|\partial^2 T|^2 \gg |\partial^4 T|$ , therefore, the third and higher order terms in Eq.(21) can be neglected (see [10] for full description). Therefore, inserting Eq.(21) in Eq.(10) and simplifying, it follows the geometric optics approximation to the amplification factor for the PM lens model [1, 10]:

$$F(w, y)_{\text{Geom}} = |\mu_+|^{1/2} - i|\mu_-|^{1/2} e^{iwt_d} \quad (22)$$

where  $\mu_{\pm} = dx_{\pm}/dy = 1/2 \pm (y^2 + 2)/y\sqrt{y^2 + 4}$  is the magnification of each image from the lens equation Eq.(12), and  $t_d = y\sqrt{y^2 + 4}/2 + \ln((\sqrt{y^2 + 4} + y)/(\sqrt{y^2 + 4} - y))$  [1, 11]. Also, since the amplification factor is complex, a *phase* will be associated with the oscillatory effect of the magnification. From Eq.(22) we can determine the magnitude and phase of the amplification factor as follows[1, 3]:

$$|F(w, y)_{\text{Geom}}| = \sqrt{\frac{y^2 + 2 + 2 \sin wt_d}{y\sqrt{y^2 + 4}}} \quad (23)$$

$$\theta_F = -i \ln \left( \frac{F(w, y)}{|F(w, y)|} \right) = \arctan \left[ \frac{-|\mu_-|^{1/2} \cos wt_d}{|\mu_+|^{1/2} + |\mu_-|^{1/2} \sin wt_d} \right] \quad (24)$$

In Eq.(23) it is possible to see that as the source position tends to perfect alignment ( $y \rightarrow 0$ ), a singularity is found, where the amplification factor diverges to infinity. This is not the case though, since it is not a physical description, instead the maximum value at  $y = 0$  is obtained

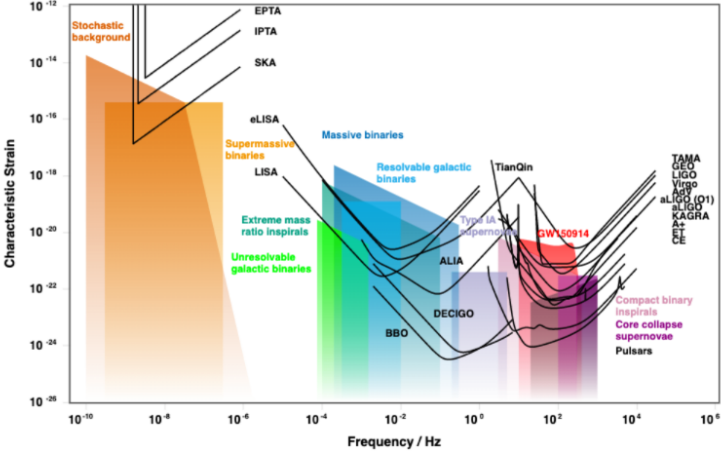


**Figure 5:** Characteristic Strain against frequency of a number of sources. Rotating neutron stars are located in the frequency range between 10-1000 Hz, where only some detectors are sensitive enough, such as ET, CE, and Advance LIGO and VIRGO. Source of image [17].

from Eq.(18) for  $w \gg 1$  [10]. Following the same calculations, one can find the amplification factor for the SIS model, which takes the following form:

$$F(w, y) = \begin{cases} |\mu_+|^{1/2} - i|\mu_-|^{1/2}e^{iwt_d} & \text{for } y \leq 1 \\ |\mu_+|^{1/2} & \text{for } y \geq 1 \end{cases} \quad (25)$$

where  $\mu_{\pm} = \pm 1 + 1/y$  and  $t_d = 2y$  [1, 4]. Figure 4 shows the dimensionless frequency parameter as a function of radiation frequency,  $f$ , for fixed lens masses. In this case we show three lenses: Sagittarius A\* ( $M = 2.6 \times 10^6 M_{\odot}$ ) [6], M31 galactic center black hole (GCBH) ( $M = 1.4 \times 10^8 M_{\odot}$ ) [15] and M22 globular cluster (GC) ( $M = 10^3 M_{\odot}$ ) [3]. For continuous gravitational wave sources, such as fast rotating NSs, with frequency between 1 - 1000 Hz, both GCBH for the Milky Way and the Andromeda galaxy will result in the use of the geometric optics limit (as  $w \approx 10^3 - 10^5$ ). For the globular cluster M22, in the same frequency region, the wave optics limit is more appropriate (as  $w \approx 10^{-1} - 10^2$ ). The grey area in Fig.4 represents  $w \geq 10^2$ , above which the geometric optics limit region well describes the high frequency gravitational lensing phenomena. In the paper [16], the value  $2\pi f t_d = 1$  was used to distinguish the regions where the geometric optics approximation well describes the lensing optics. This is a bit too optimistic, as contributions from the wave optics limit still contribute for  $w > 1$ . For this reason, we have adopted a value of  $w \geq 100$  for when the geometric limit is usable.

### 3. Continuous gravitational waves lensed by Sag A\*

#### 3.1. The nature of continuous gravitational wave sources

The main sources of continuous GW radiation is expected to be rotating *neutron stars* (NSs), but this is still uncertain since continuous gravitational waves have yet to be detected. These are the best candidates since their long lived radiation allows for a longer integration time. The continuous gravitational radiation from NSs is believed to be generated by intrinsic non-axisymmetry from residual crust deformation [18] or from the presence of a non uniform distribution of the high magnetic field [19]. Also, NSs are believed to emit gravitational waves at twice their rotational frequency, hence characterizing this radiation will allow us to constrain the rotation frequency of the NS, which is an important factor describing the compact object (together with the spin down rate) [18, 19]. Furthermore, rotating NS in our galactic bulge

are estimated to span the frequency range from 0.1 - 1000 Hz [20], which corresponds to the frequency range of VIRGO and LIGO detectors [21], and technological upgrades of these detectors (AdVirgo and aLIGO) will further increase the characteristic observable strain [17], which will allow the detection of even smaller characteristic strains. Future detectors such as the Einstein Telescope and the Cosmic Explorer will further extend the strain sensitivity. Also, the detection of continuous gravitational waves from rotating NSs would yield important information on the structure and equation of state of these compact objects [18]. Neutron stars located behind the dust filled galactic center are optically invisible, therefore, observations of the continuous gravitational radiation are the only means of their detectability [18, 21, 22]. Starting from this concept, studying the diffraction effects of gravitational waves as they pass near a massive lens will further improve the observability by amplifying the radiation through the interference pattern, shown in Fig.2. Following this section, a comprehensive analysis of the lensed continuous gravitational waves will be carried out with radiation frequency of 10 and 100 Hz.

### 3.2. Interference pattern

Gravitational lensing of rapidly rotating NSs located behind Sag A\* has already been analyzed by [21, 23]. We will base our analysis on these compact objects and estimate their amplification, using the lensing parameters of Sag A\* ( $M \approx 2.6 * 10^6 M_{\odot}$ ) located at a distance of  $D_L = 8$  kpc [6]. These continuous GW sources will have a very high dimensionless frequency parameter, thus putting them in the geometric optics limit (sources with  $f = 1 - 1000$  Hz will have  $w \geq 100$ ). Starting from Eq.(23), the amplification factor will have a radial symmetry (no angular component is present), therefore by changing  $y$  into the radial component, as  $R = \sqrt{z^2 + y^2}$ , which are cartesian coordinates at the source plane<sup>3</sup>, we can make a 2D plot showing the radial amplification factor values. The amplification factor plotted in a 2D radial plot for a 100 Hz and 10 Hz are shown in Fig.6 and Fig.7 respectively. The lensing parameters used in Fig.6 and Fig.7 are:  $M \approx 2.6 * 10^6 M_{\odot}$ ,  $D_L = 8$  kpc,  $D_S = 12$  kpc. The maximum central amplification for the two figures has been reduced by a factor of 10 to clearly show the interference pattern around the central cusp ( $F_{\max} = 318$ ) and ( $F_{\max} = 110$ ).

Due to the high oscillatory behavior (large dimensionless frequency parameter), Fig.6 and Fig.7 were numerically difficult to evaluate as the amplification factor depends strongly on the grid spacing over the 2D plots (*sign* problem in lattice QCD) [24]. To get around this, a table-approach method was adopted, where a 1D radial amplification was computed and compared with the 2D radial values. Also, Fig.6 and Fig.7 were plotted across  $y = -0.5$  and  $y = 0.5$  of dimensionless source position, allowing us to differentiate the amplification fringes between one another. By definition, any sources inside one Einstein angle over the source plane will have a magnification greater than unity. This is shown by using Eq.(23), where we can solve for the amplification factor in the eikonal limit (no interference parameter) at distance corresponding to one Einstein radius on the source plane, as follows:

$$|F(1)| = \sqrt{\frac{y^2 + 2}{y\sqrt{y^2 + 4}}} = 1.15 \quad (26)$$

where we have used the geometric amplification and set the time delay function equal to zero (classical approach to amplification) [21, 24]. Already at  $y = 1$ , the amplification would reach an average of 15% above unity, thus showing how quickly the amplification factor falls as the source is located further away from perfect alignment. Quantitatively speaking, the amplification factor decreases by about 94% over the second spatial fringe. Also, for a distance of  $D_S = 12$  kpc,

<sup>3</sup> Note:  $x$ - $y$  coordinates span the galactic plane, instead the  $z$ -coordinate spans the galactic height.

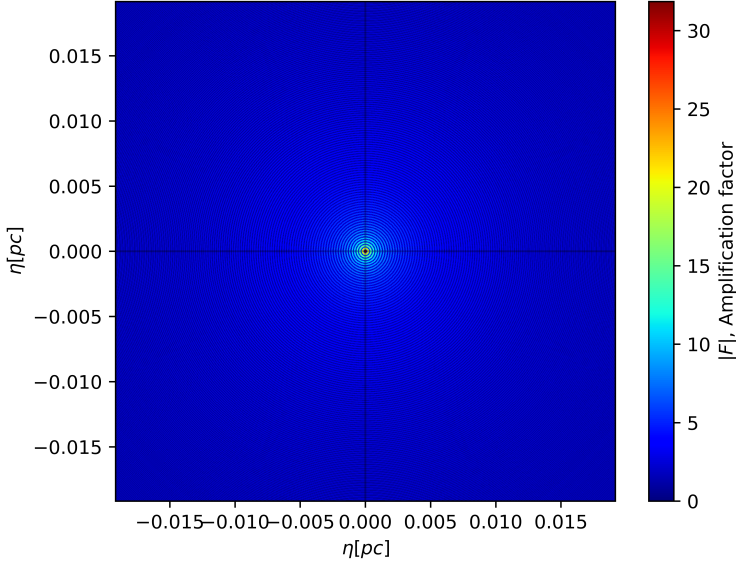


**Figure 6:** 2D plot of amplification factor with parameters:  $f = 100$  Hz,  $M = 2.6 \times 10^6 M_\odot$ ,  $D_S = 12$  kpc. The axis are the positional values of the source at a distance  $D_L = 8$  kpc over a dimensionless source position range of  $y = \pm 0.5$ .

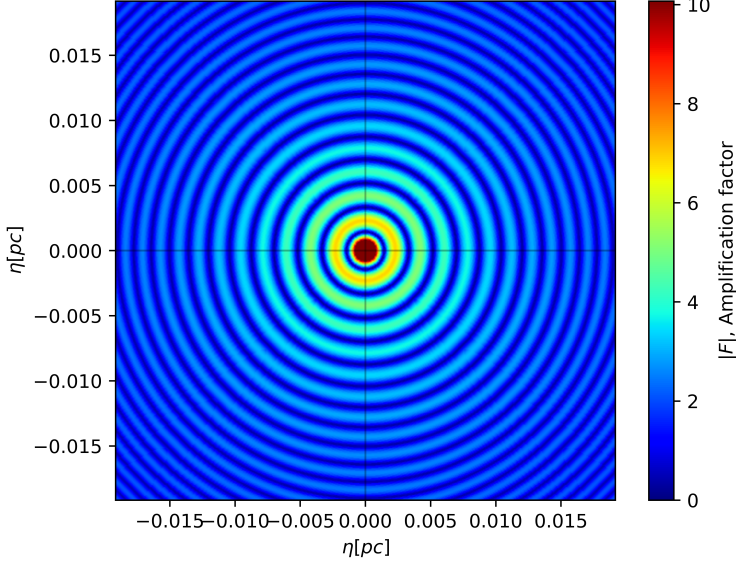


**Figure 7:** 2D plot of amplification factor as in Fig.6, but with  $f = 10$  Hz

the corresponding Einstein radius will be  $R_E = \theta_E D_L = 0.0297$  pc. Inserting the value in the dimensionless source position and solving for the physical vector position of the source, it follows  $\eta = |y|R_E D_S/D_L = 0.0446$  pc. Therefore, high amplifications of the signal will occur at relatively small astronomical scales. This is also discussed in [21], where they show typical galactic bulge NSs will have a strain amplitude of  $h_0 = 3 \times 10^{-26}$ , and by taking into account the micro-lensing effect, for distances much less than one Einstein radius, a maximum amplitude will correspond

to  $h_{max} = F(\eta < R_E)h_0$ , where the amplification can be as high as a 10, thus facilitating the detectability [24, 25]. To have a more complete understanding of the observability of these amplified continuous sources, a more dynamical picture of the system has to be considered. To do so, relative velocities of the the observer (Earth) and source (NSs) have to be considered to understand how the amplification factor would modulate the continuous signal. The next section will look into understating how relative motions effect the detectability of these signals and how different sources modulate the signal depending on their frequency.

### 3.3. Point mass lens with relative motion

In the previous section, we considered a stationary point source emanating continuous gravitational waves, being lensed by Sag A\*. We showed how the gravitational radiation will be amplified depending on the relative positions of source-lens-observer. In reality, the observer, lens, source are all moving with respect to each other, therefore the relative velocities have to be taken into account. Also, in a more accurate representation, the observer would trace out a line as it moves in the source plane in Fig.6 which would represent the observer moving relative to the lens and the source. This gives us an idea of how the gravitational wave detected will change in amplification over an observing time, and hence allow us to estimate the lensing parameters. Present and future GW detectors need a relative long integration time to detect with a certain degree of accuracy the incoming gravitational wave [1, 3, 21, 24], therefore, an estimate of the time-scales to cross the interference pattern is needed. To do so, we consider the peculiar motions of the lensing system to retrieve the effective motion of the source with respect to the lens (applicable for galactic sources), as follows:

$$\mathbf{v}_{\text{eff}} = \mathbf{v}_S - \frac{D_S}{D_L} \mathbf{v}_L + \frac{D_S - D_L}{D_L} \mathbf{v}_{\text{obs}} \quad (27)$$

where  $\mathbf{v}_S$ ,  $\mathbf{v}_L$  and  $\mathbf{v}_{\text{obs}}$  are the source, lens and observer velocities respectively. Therefore, the time scale of observability would be  $t_f = R_E/v_{\text{eff}}w$  [3, 26]. Assuming stationary source and lens, frequency of  $f = 10$  Hz, and the relative distances discussed in Section 3.2,  $t_f \approx 30$  days (time scale for observability of fringes). Fortunately, this amplitude modulation can be discerned from the modulation arising from Earth orbital and rotational motion (which as time scale of about 1 day) [3, 24]. For  $f = 100$  Hz,  $t_f \approx 3$  days, hence Earth's orbital and rotational motion have to be considered in the signal modulation.

From Eq.(27), it is also possible to compute the Einstein crossing time, defined as follows [3]:

$$t_E \approx 37.4 \text{ days} \sqrt{4 \frac{D_L}{D_S} \left(1 - \frac{D_L}{D_S}\right) \left(\frac{M}{M_\odot}\right)^{1/2} \times \left(\frac{D_S}{8 \text{kpc}}\right)^{1/2} \times \left(\frac{v_{\text{eff}}}{200 \text{km/s}}\right)^{-1}} \quad (28)$$

The Einstein crossing time is the time it takes for the observer to cross the distance of one Einstein radius on the source plane with velocity  $v_{\text{eff}}$ . For an effective velocity of 200 km/s and the lensing system considered, the Einstein crossing time will be of the order of  $t_E \approx 64400$  days  $\approx 176$  years. Figure 8 shows the amplification curves plotted over time axis (in units of days) for different radiation frequency being lensed by Sag A\* with  $y_0 = 0.5$  and  $D_S = 12$  kpc. To quantify the motion of the observer over the interference, we consider the dimensionless radial position changing in time, as follows:

$$y(t) = \sqrt{\left(\frac{t - t_0}{t_E}\right)^2 + y_0^2} \quad (29)$$

where  $y_0$  is the closest approach distance and  $t_0$  is the time when this occurs during the observation. Inserting Eq.(29) in Eq.(23) the amplification factor can be described as a function

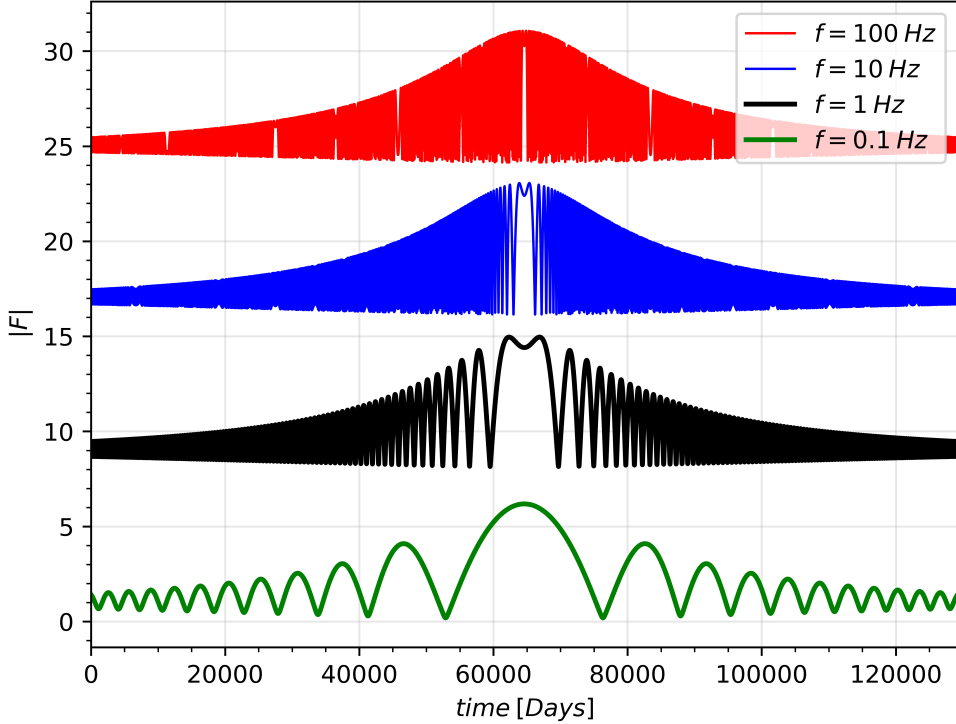


**Figure 8:** Amplification factor for different values of radiation frequency with fixed lens mass (Sag A\*) during a crossing at  $y_0 = 0.5$ . The curves were shifted from one another to show more clearly the features from each amplification: red curve 100 Hz, blue curve 10 Hz, black curve 1 Hz, green curve 0.1 Hz (value of the shift is 8). The  $x$  axis runs from 0 to 2 Einstein crossing times with closest approach at 1 Einstein crossing time.

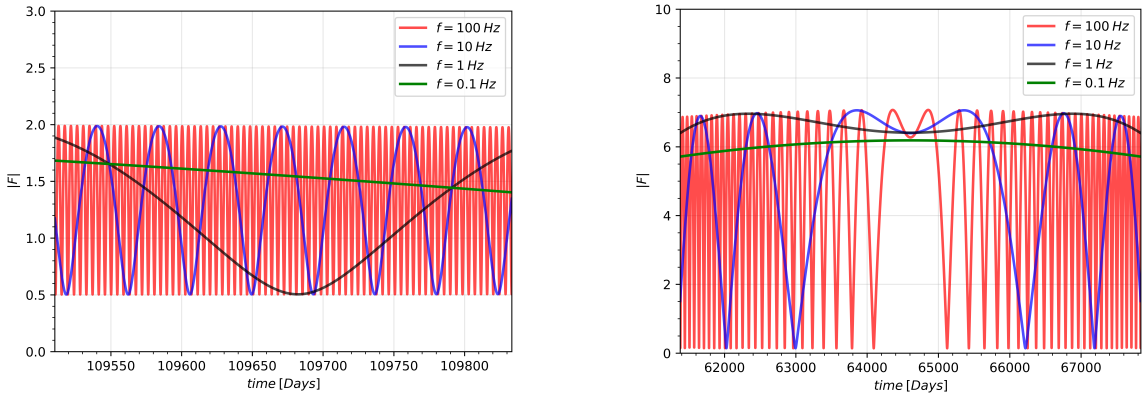


**Figure 9:** *Left:* Zoomed in section of Fig.8 far away from the closest approach, over a period of  $\approx 1$  year . *Right:* Zoomed in section of Fig.8 over closest approach, over a period of  $\approx 24.5$  years.

of observing time,  $t$  [3, 26, 24]. Figure 8 shows different crossings for  $y_0 = 0.5$  and  $t_E = 64400$  days. The plot spans 2 Einstein crossing times, therefore the time of closest approach is  $t_0 = t_E$ . The respective frequencies are: red curve 100 Hz, blue curve 10 Hz, black curve 1 Hz and green curve 0.1 Hz. The shape of the amplification curve is overall constant over 1 to 100

Hz. For lower frequency radiation, the geometric optics limit fails to describe the amplification curve, since  $w < 100$  at  $f = 0.1$  Hz (see Fig.4). Therefore, the wave optics should be used for these type of sources (i.e. WD-WD binaries, slow rotating neutron stars). Figure 9(left) shows the amplification factors in Fig.8 overlapping, away from the central peak of closest approach, spanning roughly 1 year of observation time. From this it is possible to observe how the 100 Hz frequency amplification peaks are very close together compared to the lower frequency curves, instead the 0.1 Hz varies by only approximately 10% over the observation time. Figure 9(right) shows a zoomed in plot of the amplification factor from Fig.8, just as before, but here the section of closest approach is shown. The time axes spans about  $\approx 24.5$  years, showing how slowly the amplification factor modulation would be observed for different frequencies over a long integration time. In fact, the change in amplitude for 0.1 Hz sources would be hardly noticeable. On the contrary, the 100 Hz amplification curve is well sampled along the integration time, showing a constant amplification oscillation in the period of several years. This is suitable for long integration time scale as it would provide us with a constant amplification modulation and, hence allow us to estimate lensing parameters more precisely.

#### 4. Probability of NSs being amplified above a certain threshold

##### 4.1. NS probability distributions

To fully describe the feasibility of detecting GWs from rotating NSs located in the galactic bulge, it would be appropriate to characterize the distribution of said sources in a statistical manner. To do so, we start from three NS spatial distributions given by [21, 27, 28], as follows:

$$p(R)_{\text{P90}}dR = \alpha_R \frac{R}{R_{\text{exp}}^2} e^{-\frac{R}{R_{\text{exp}}}} dR \quad (30)$$

where Eq.(30) (referred to as P90) is a probability density function of NSs defined between  $R$  and  $R + dR$ , with  $R_{\text{exp}} = 4.5$  kpc and  $\alpha_R = 1.0683$  [27];

$$p(R)_{\text{F06}} = \frac{1}{\sqrt{2\pi\sigma^2}} e^{-\frac{[R-R_{\text{peak}}]^2}{2\sigma^2}} \quad (31)$$

where Eq.(31) (referred as F06) is a probability density function of NSs, with mean  $R_{\text{peak}} = 7.04$  kpc and  $\sigma = 1.83$  kpc;

$$\rho(R)_{\text{CB98}} = \left( \frac{R}{R_0} \right) e^{-\frac{\beta[R-R_0]}{R_0}} \quad (32)$$

where (32) (referred as CB98) is a number density function of NSs, with  $R_0 = 8.5$  kpc,  $\beta = 3.53$  and  $\alpha = 2$ . To extract the radial probability density function (PDF) from Eq.(32), we used the following equation [27]:

$$p(R)dR = \frac{R\rho(R)dR}{\int_0^\infty R\rho(R)dR} \quad (33)$$

Starting from Eq.(30), Eq.(31), Eq.(32) we can assume radial symmetry and extend the distribution to the galactic plane coordinate system [27, 28]. As far as the  $z$  component is concerned, [28] gives a distribution over the galactic altitude described by a gaussian function, centered at  $z = 0$  (galactic plane) as follows :

$$p(z) = \frac{1}{\sqrt{2\pi}h_{\text{int}}} e^{-\frac{z^2}{2h_{\text{int}}^2}} \quad (34)$$

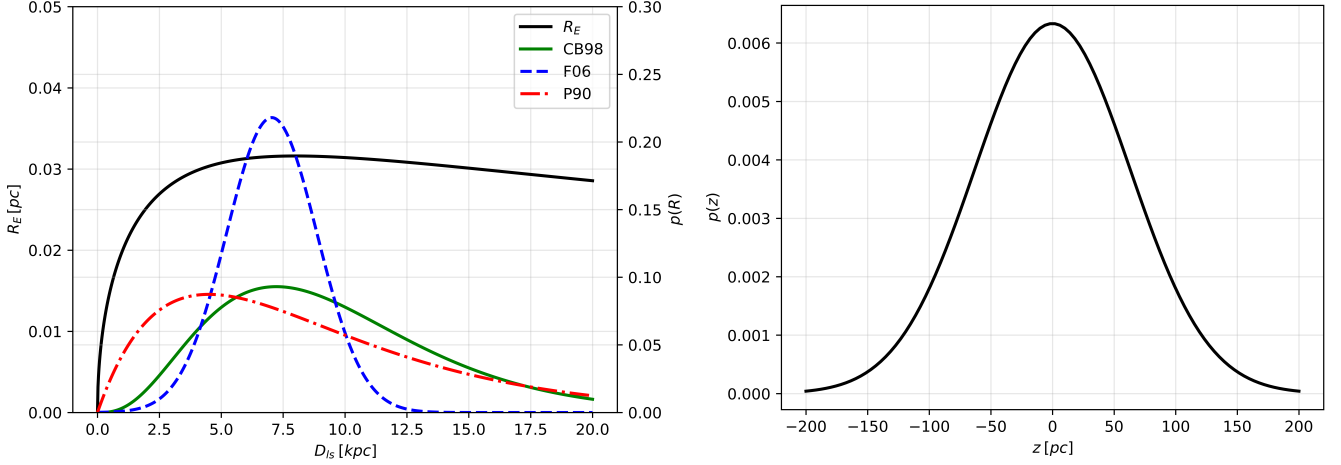


**Figure 10:** *Left:* Probability density functions of galactic bulge NSs described over 0 to 20 kpc from the GC. The names of the curves correspond to the authors mentioned in [27]. The black solid curve represents the Einstein Radius as  $D_{ls}$  increases, where the maximum lies near the maxima of the distributions, suggesting high lensing probability of NSs, due to the greater lensing scale. *Right:* Probability density function in the  $z$  axes, which spans the height of the galaxy.

where  $h_{int} = 63$  pc is the scale-height. This height distribution is in good agreement with *Hipparcos* data, though the galactic halo is not considered [28]. Fig.11(left) shows the probability functions mentioned earlier together with the Einstein Radius,  $R_E$ . The plot shows where the highest probabilities of finding NSs behind the GC as a radial function. The maximum Einstein radius lies in the neighborhood of the maxima of the population distribution, suggesting a high probability of NSs will lensed by Sag A\*. Fig.11(right) shows the vertical distribution of NSs above and below the galactic plane given by Eq.(34). To estimate the number of NSs located behind Sag A\*, but also inside the lensing scale length, we first converted the 1D PDFs into 2D distributions, spanning the galactic bulge area(  $20 \times 20$  kpc) [27].

The lensing scale is defined as the dimensional source position,  $\eta = y\theta_E D_S$ , which increases as  $D_S$  increases. To detect the fringes for a point mass lens, a criteria of detectability has to be followed [3]: 1)  $w > 1$  to have enough variation in the amplification of the signal; 2)  $y < 3$  to detect fringes before they are damped; 3)  $\Delta t > t_f$  to see the fringe pattern, where  $\Delta t$  is the observing time length. Therefore, we considered a maximum scale length of  $y = 3$ , which is the maximum scale length sources can be located to produce amplification fringes before they are damped.

#### 4.2. Number of sources lensed by Sag A\*

To estimate the number of NSs lensed by Sag A\*, we start by multiplying the fraction obtained by integrating the PDF of NSs over the desired boundaries and multiplying it by the total number of sources, which is of the order of  $10^9$  [27, 28, 21, 3, 29]. To do so, we assume the fraction of sources located behind Sag A\* with respect to the total number is equal to the fractional value obtained by integrating over pdfs in the  $xy$  (galactic) plane and  $yz$  (source) plane. In our case, the source plane in Fig.6 spans the  $yz$  plane, therefore, these boundaries will have to vary as we move in the  $x$  direction, as  $\pm\eta(3, x)$ . The number of NS sources located in the lensing scale is then computed as follows:

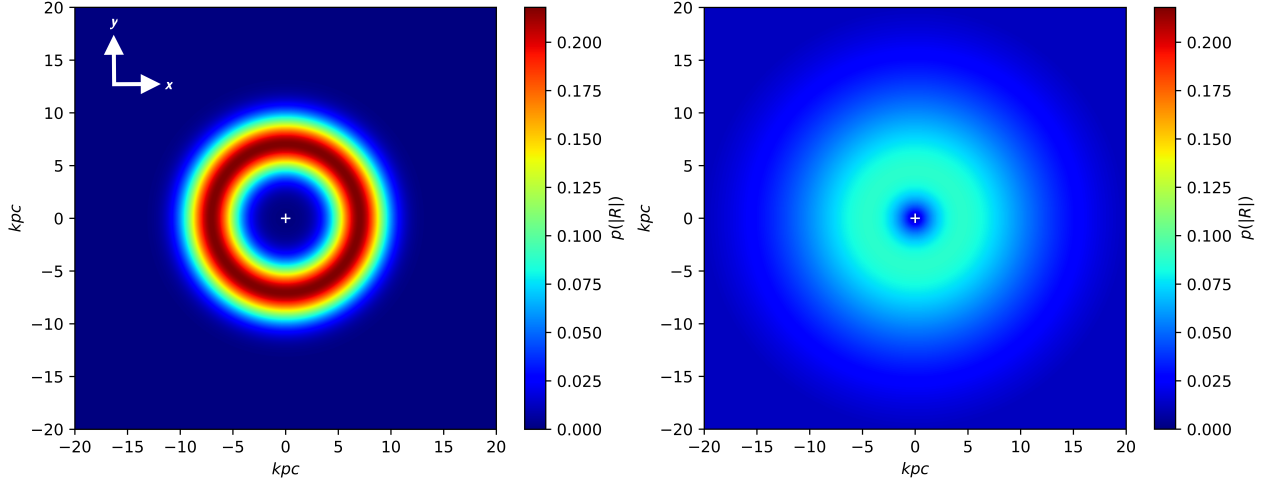


**Figure 11:** *Left:* NS radial probability density function plotted over a 2D plot (F06 Model). The white cross in the center corresponds to the origin of the GC (Sag A\*). *Right:* NS radial probability density function plotted over a 2D plot (P90 Model).

$$N_{\text{sources}} \approx 10^9 \frac{\int_0^{20} \int_{-\eta(3,x)}^{\eta(3,x)} \int_{-\eta(3,x)}^{\eta(3,x)} p(x,y)p(z)dxdydz}{\int_{-\infty}^{\infty} \int_{-\infty}^{\infty} \int_{-\infty}^{\infty} p(x,y)p(z)dxdydz} \quad (35)$$

where the denominator normalizes the distributions. Using Eq.(35), we can insert Eq.(30), Eq.(31), Eq.(32), combined with Eq.(34) to obtain the total number of NSs located behind Sag A\* for each PDF respectively. Figure 12 shows the PDFs over a  $20 \times 0.004$  kpc region behind Sag A\*, form the observer prospective. Different lines show how wide the search boundaries are for dimensionless source values of  $y = 1$ ,  $y = 3$  and  $y = 10$ .

For  $y = 3$ , an average of  $N_{\text{P90}} \approx 12 \pm 3$ ,  $N_{\text{F06}} \approx 15 \pm 3$  and  $N_{\text{CB98}} \approx 13 \pm 3$  sources were obtained respectively. The errors on the obtained results correspond  $\sqrt{N}$  rounded to an integer value.

After having computed the number of NSs we expect to be lensed by Sag A\*, the next step would be to quantitatively estimate what would the maximum amplification be by randomly placing these sources, both in physical and frequency space. To do so, we run a Monte Carlo (MC) simulation where frequency,  $f$ , and source position,  $y$ , are allowed to vary, keeping the mass of the supermassive black hole constant.

## 5. Monte Carlo simulation of amplification factor, $F(w, y)$

To run the MC simulation, we first have to characterize our priors on frequency and source position. To do so, we considered a uniform prior on dimensionless source position ranging from 0 to  $+3$ . For the radiation frequency, we used a pulsar period distribution given by [20], which is described by a gamma function as follows:

$$f(P) = G_0 \left(\frac{P}{m}\right)^{a-1} e^{-\frac{P}{m}} \quad (36)$$

where  $G_0$  is a normalization constant (dependent on  $a$ ),  $P$  is the period of rotation of the pulsar and  $a$  and  $m$  are fitting constants. Following, model B in [20], the fitting parameters are  $a = 2.6$  and  $m = 0.36$ . Therefore, we can draw random frequency values from the gamma probability distribution function defined for a frequency range range of  $0.23 < f < 20$  Hz [20] (recall,  $P = 1/f$ ). To simulate the number of sources, we randomly draw from a Poisson

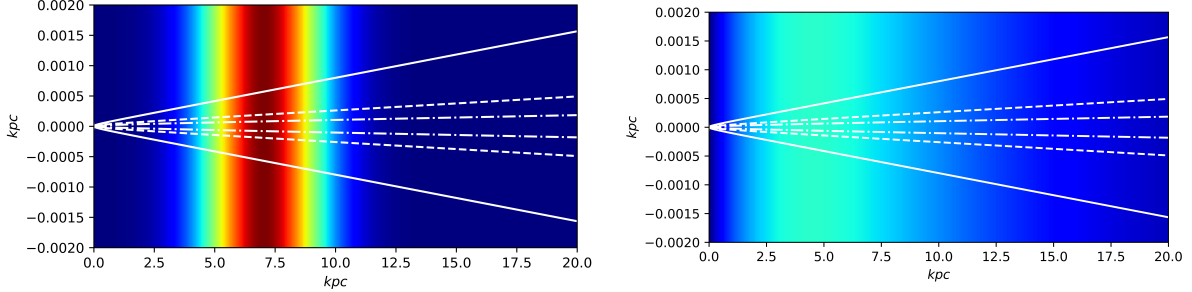


**Figure 12:** *Left:* cross section of 2D plot spanning an area of  $20 \times 0.004$  kpc, observer (Earth) is located at about 8 kpc on the left side of the galactic center. The white solid-dot line is the lensing scale length at the source position (i.e.  $\eta$ ). *Right:* Zoomed in version behind Sag A\*. The white lines represents the dimensional scale lengths as a function of  $y = 1$ ,  $y = 3$  and  $y = 10$  for the “dotted”, “segmented” and “solid” lines respectively.

distribution with a mean of  $\lambda_{F06} = 15$  (highest mean obtained in Section 4.2). From this, we run the following algorithm: we select  $N$  random sources from the Poisson distribution, with random frequency ( $w$  randomly drawn from the gamma function, Eq.(36)) and random source positions; we then select the source which gives the maximum amplification over the  $N$  draws, as  $F = \max[F(f_{\text{random}}, y_{\text{random}})]$ . For frequencies with  $w \geq 100$  (i.e.  $f \geq 1$  Hz), the amplification factor was computed using the geometric optics limit, otherwise, wave optics function was used. Figure 13 shows  $10^6$  realizations of the MC simulation, shown through a corner plot where the results of amplification factor with corresponding source position and radiation frequency are plotted. In the source position-frequency plot, the radial amplification fringes are clearly visible for  $y < 0.3$  and  $f < 1.5$  Hz (also observed in [24]). The frequency distribution plotted on the bottom right in Fig.13 reflects the gamma distribution, Eq.(36), suggesting  $F_{\text{max}}$  is not strongly dependent on frequency, since the random selection of frequencies was not constrained by the selection of the maximum amplification factor. On the contrary,  $F_{\text{max}}$  is strongly constrained by the source position, consistent with [3].

The median amplification factor obtained from the distribution occurs at  $|F_{\text{max}}|_{\text{median}} = 2.67$  and the mode at  $|F_{\text{max}}| = 1.85$ . To compute the probability of a source being amplified above a certain threshold, integrate the maximum amplification factor  $p(|F|)$ , after correctly normalizing it. As for example, the probability of finding a source amplified by a factor of 10 is  $p(|F| \geq 10) = 4.79\%$ , instead for amplifications greater than 2,  $p(|F| \geq 2) = 71.66\%$ . This means that, over a range of possible realizations of randomly positioned sources behind Sag A\*, 5% of the time we would expect the source to be amplified above a factor of 10, therefore an amplification of one order of magnitude is not impossible. Two important notes on Fig.13 : first, the amplification factor for any source gets highly damped as  $y \rightarrow 3$  (i.e.  $F \rightarrow 1$ ), consistent with [3, 4]; secondly, a degeneracy arises between source position and frequency, clearly visible for low amplification values. This suggests that, as long as there is no perfect alignment, which it was shown to be very improbable in [21], selected sources with any position and frequency values can have the same maximum amplification factor. For  $F_{\text{max}} > 10$  and source positions close to 0.1, the amplification factor begins to be strongly constrained by the radiation frequency. This is due to the fact that, close to perfect alignment, the peak of amplification factor is solely determined by the dimensionless frequency parameter,  $w$ . Therefore, detections of highly amplified continuous GWs will, in principle, allow for a direct measurement of the lensing mass, which in this case would be Sag A\*.

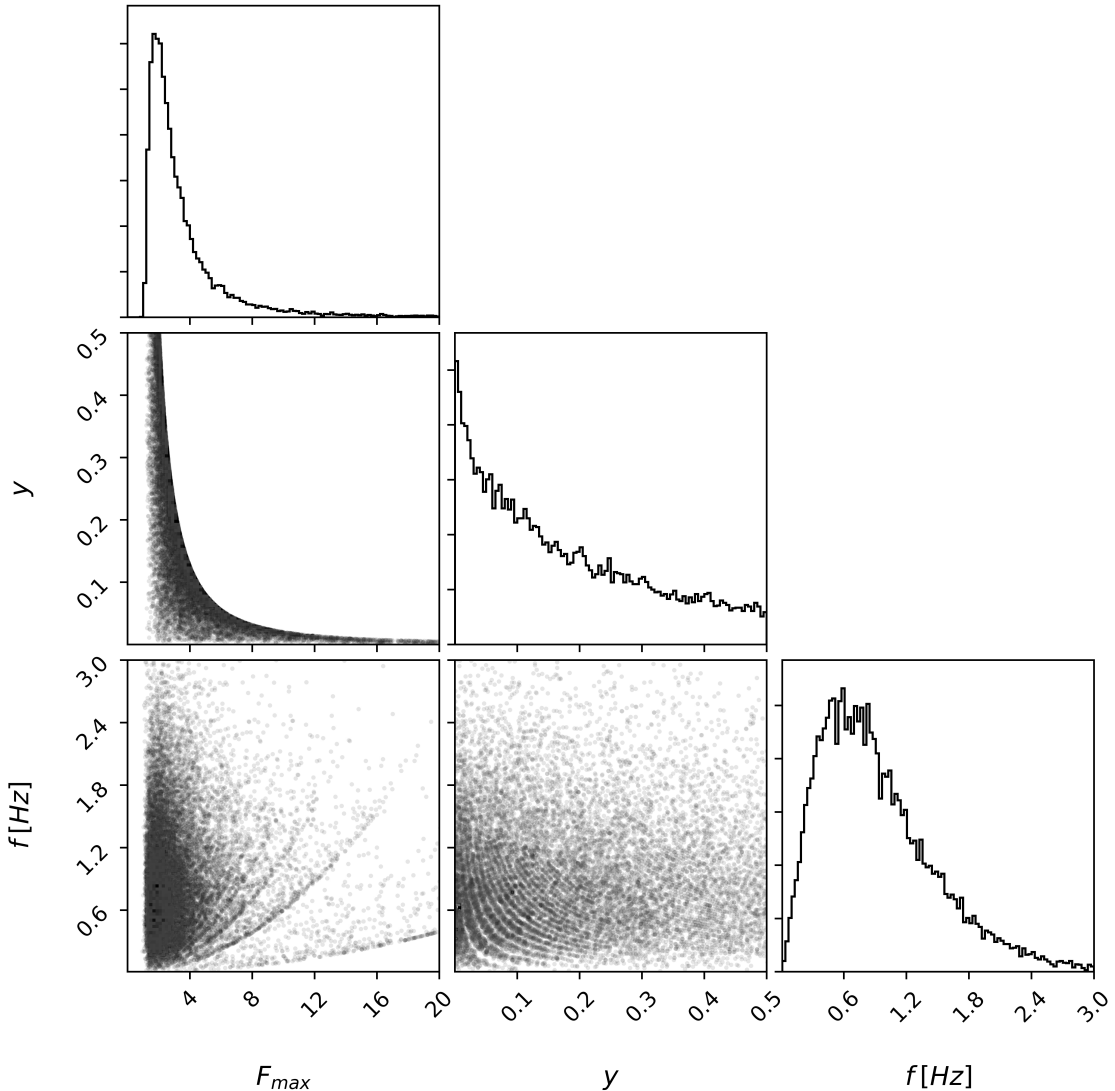


**Figure 13:** Corner plot showing the 3D realization of the MC simulation with maximum amplification factor, source position and radiation frequency. The amplification fringes are clearly visible in the frequency space, instead less clearer in the source position frequency plot.

## 6. Conclusion and Future Work

In this report we have quantitatively assessed how continuous GW waves from NSs can be amplified by a massive compact object, such as the galactic center black hole in our galaxy. In the first part we used formalism outlined in [1] to solve the amplification factor of a GW as it gets lensed by a compact object both in geometric and wave optics regimes. For NSs located in the galactic bulge behind Sag A\*, with respect to the observer (Earth), the geometric optics limit describes the amplification of the gravitational radiation appropriately for the considered sources. As the radiation gets lensed, an interference pattern arises due to the wave nature of the GWs. These spatial fringes are clearly visible in the 2D radial plots in Section 3, for sources with frequency of 100 and 10 Hz, shown in Fig.6 and Fig.7 respectively. These plots show how quickly the amplification decays the further away a source is from perfect alignment. In Section 3.3 we considered the relative motions of the source-lens-observer and, specifically, how we would

detect this modulation arising from the differential amplification factor over spatial coordinates. Here we considered a simplistic approach, where the lens object was kept static and only the observer (or the source) was allowed to move. In this case, the dimensionless spatial coordinate  $y$  was replaced with the more appropriate parameter  $\sqrt{((t - t_0)/t_E)^2 + y_0^2}$  [26]. In the case of galactic NSs, the distances can be regarded as Euclidian, therefore no consideration of space time curvatures are needed [3]. The reason why we are selecting isolated NSs to observe is due to their long lived continuous gravitational waves at frequencies between 1 Hz and 1000 Hz, which are the frequency range of LIGO and third generation ground based detectors, such as the Einstein Telescope (ET) and the Cosmic Explorer (CE). Due to the low characteristic strain of these sources, detecting them with enough SNR is challenging. The amplification factor offers a way to boost the signal up by a factor of 10, which would help in the detection these NSs, since it is not possible to observe them with other means. By plotting the amplification factor over time, the modulation from different frequency signals are observed. Specifically, for sources which are far away from perfect alignment, 100 Hz sources would have to be well sampled during integration time, due to the low modulation. Sources with 0.1 Hz will show only a difference in amplification by 10% over the course of 1 year of observational time.

In Section 4, a quantitative analysis of how many sources we would expect to be lensed is carried out. To do so, spatial probability distributions of NSs were used to plot 2D representations of where these sources are located in the galactic bulge (spanning  $20 \times 20$  kpc) [27]. Also, a height distribution function was used to describe the distribution above and below the galactic plane. To estimate the number of lensed NSs behind Sag A\*, we consider the actual physical distance parameter,  $\eta(y, D_S) = y\theta_E D_S$ . Therefore, the boundaries in the  $zy$  plane are  $\pm\eta(3, D_L + x)$ , since any source located outside  $y = 3$  will have a damped amplification (i.e.  $F = 1$ ) [3]. From this we can integrate the PDFs over these boundaries and from 0 to 20 kpc in the  $x$  direction. After correctly normalizing the PDFs, the results of integration represent the fraction of stars that would be present in our considered section, from which we then multiply the amount of NSs we believe to be in the GB,  $10^9$ . The expected number of sources was found to be  $N_{F06} = 15 \pm 3$ ,  $N_{P90} = 12 \pm 3$  and  $N_{CB98} = 13 \pm 3$  for the respective NS population distribution. These values were then used to carry out a Monte Carlo simulation for quantitatively estimating what would be the best case scenario in detecting an amplified gravitational wave signal. To do so, we first set a uniform prior for the dimensionless source position, instead the prior on frequency was set using a gamma distribution given by [20]. We then drew  $N$  number of sources from a Poisson distribution with average  $\lambda = 15$  and selected the maximum value between them, with the respective frequency and source position. The registered mode of the amplification factor was found to be  $F_{\max} = 1.85$ . Figure 13 shows the result of  $10^6$  realization of our MC simulation. Results show a uniform distribution in frequency values, suggesting that the maximum amplification factor is weakly dependent on frequency. However, source position is correctly constrained by the amplification factor, as we would expect the highest values to be located near perfect alignment ( $y = 0$ ). For  $F_{\max} > 10$  and source positions close to 0.1, the amplification factor was found to be dependent on the radiation frequency, since close to perfect alignment, the peak of amplification factor is solely determined by the dimensionless frequency parameter,  $w$ . Unfortunately, a degeneracy also arises over the source position-amplification plot shown in Fig.13. where the same maximum amplification occurs for different source positions. Therefore, as long as there is no perfect alignment (highly improbable [21]) any pulsar with frequencies of the order of 1 - 10 Hz behind Sag A\* would have the same chance of maximum amplification.

Future work will look into extending this analysis of NSs being lensed by different compact objects, such as SIS models (i.e. globular cluster, M22) and/or NFW(Navarro-Frenk-White) models (dark halo) to understand how the maximum amplification distribution changes for different lenses. Different source distributions would be used to quantitatively estimate how

many sources would be in the lensing space and, moreover, how many different types can be considered. Therefore, a new rotational frequency distribution will be used spanning all NSs, not only pulsars. Other sources could be WD-WD binaries, which are expected to be observed by the next space based detectors, such as LISA, which would provide us a better spatial distribution of these continuous GW sources, giving us an idea of how many we would expect to be lensed. Future considerations will also look at investigating the role of the angular momentum of the lensing object and how this would effect the lensing system and interference pattern. This has already been discussed by [7], where they account for the spin of Sag A\* (dimensionless spin parameter  $a$ ). They prove the system only changes trivially, by adjusting the dimensionless source parameter as  $\tilde{\mathbf{y}} = \mathbf{y} + \alpha$ , where  $\alpha = \mathbf{n} \times \mathbf{J}/\xi_0$  is the angular momentum vector normalized by the impact parameter. In conclusion, the chance of observing NSs in the galactic bulge being lensed above a certain amplification threshold is plausible. Hopefully, with the upcoming upgrades of the detectors, these elusive continuous GWs might be able to be observed, and using the amplification of compact lenses, would raise our chances in detecting them.

## References

- [1] R. Takahashi and T. Nakamura, “Wave effects in the gravitational lensing of gravitational waves from chirping binaries,” *The Astrophysical Journal*, vol. 595, pp. 1039–1051, Oct 2003.
- [2] A. Einstein, “On the General Theory of Relativity,” *Sitzungsber. Preuss. Akad. Wiss. Berlin (Math. Phys.)*, vol. 1915, pp. 778–786, 1915. [Addendum: Sitzungsber.Preuss.Akad.Wiss.Berlin (Math.Phys.) 1915, 799–801 (1915)].
- [3] K. Liao, M. Biesiada, and X.-L. Fan, “The wave nature of continuous gravitational waves from microlensing,” *The Astrophysical Journal*, vol. 875, p. 139, Apr 2019.
- [4] T. R., “Quasi-geometrical optics approximation in gravitational lensing,” *A&A*, vol. 423, no. 03, pp. 787–792, 2006.
- [5] B. P. Abbott, R. Abbott, T. D. Abbott, M. R. Abernathy, F. Acernese, K. Ackley, C. Adams, T. Adams, P. Addesso, R. X. Adhikari, and et al., “Localization and broadband follow-up of the gravitational-wave transient gw150914,” *The Astrophysical Journal*, vol. 826, p. L13, Jul 2016.
- [6] F. De Paolis, G. Ingrosso, A. A. Nucita, A. Qadir, and A. F. Zakharov, “Estimating the parameters of the sgr a\* black hole,” *General Relativity and Gravitation*, vol. 43, p. 977?988, Nov 2010.
- [7] C. Baraldo, A. Hosoya, and T. T. Nakamura, “Gravitationally induced interference of gravitational waves by a rotating massive object,” *Phys. Rev. D*, vol. 59, p. 083001, 1999.
- [8] K. Yamamoto, “Path integral formulation for wave effect in multi-lens system,” 2003.
- [9] F. A. Asenjo and S. A. Hojman, “New non-linear modified massless klein-gordon equation,” *The European Physical Journal C*, vol. 77, Nov 2017.
- [10] T. T. Nakamura and S. Deguchi, “Wave Optics in Gravitational Lensing,” *Progress of Theoretical Physics Supplement*, vol. 133, pp. 137–153, 01 1999.
- [11] P. Schneider, F. Ehlers, and E. E. Falco, *Gravitational Lenses*. 1992.
- [12] N. Matsunaga and K. Yamamoto, “The finite source size effect and wave optics in gravitational lensing,” *Journal of Cosmology and Astroparticle Physics*, vol. 2006, pp. 023–023, Jan 2006.
- [13] M. Abramowitz and I. Stegun, *Handbook of Mathematical Functions with Formulas, Graphs, and Mathematical Tables*, vol. 55, n. 1972. U.S. Government Printing Office, 1970.
- [14] X.-D. Luo and W.-C. Lin, “Some new properties of confluent hypergeometric functions,” 2015.

- [15] Z. Li, Q. D. Wang, and B. P. Wakker, “M31\* and its circumnuclear environment,” *Monthly Notices of the Royal Astronomical Society*, vol. 397, no. 1, p. 148?163, 2009.
- [16] A. K. Meena and J. S. Bagla, “Gravitational lensing of gravitational waves: wave nature and prospects for detection,” *Monthly Notices of the Royal Astronomical Society*, vol. 492, no. 1, p. 1127?1134, 2019.
- [17] C. J. Moore, R. H. Cole, and C. P. L. Berry, “Gravitational-wave sensitivity curves,” *Classical and Quantum Gravity*, vol. 32, p. 015014, Dec 2014.
- [18] K. Riles, “Gravitational waves: Sources, detectors and searches,” *Progress in Particle and Nuclear Physics*, vol. 68, pp. 1–54, Jan 2013.
- [19] S. Bonazzola and E. Gourgoulhon, “Gravitational waves from pulsars: emission by the magnetic field induced distortion,” 1996.
- [20] K. Maciesiak, J. Gil, and V. A. R. M. Ribeiro, “On the pulse-width statistics in radio pulsars - i. importance of the interpulse emission,” *Monthly Notices of the Royal Astronomical Society*, vol. 414, no. 2, pp. 1314–1328, 2011.
- [21] F. De Paolis, G. Ingrosso, and A. A. Nucita, “Astrophysical implications of gravitational microlensing of gravitational waves,” *Astronomy & Astrophysics*, vol. 366, pp. 1065 – 1070, Feb 2001.
- [22] I. Yusifov and I. Kk, “Revisiting the radial distribution of pulsars in the galaxy,” *Astronomy & Astrophysics*, vol. 422, pp. 545–553, Jul 2004.
- [23] A. A. Ruffa, “Gravitational lensing of gravitational waves,” *The Astrophysical Journal*, vol. 517, pp. L31–L33, May 1999.
- [24] D. L. Jow, S. Foreman, U.-L. Pen, and W. Zhu, “Wave effects in the microlensing of pulsars and frbs by point masses,” 2020.
- [25] F. De Paolis, G. Ingrosso, A. A. Nucita, and A. Qadir, “A note on gravitational wave lensing,” *Astronomy & Astrophysics*, vol. 394, p. 749?752, Oct 2002.
- [26] B. Paczynski, “Gravitational microlensing by the galactic halo,” *Astrophysical Journal, Part 1 (ISSN 0004-637X)*, vol. 304, May 1, 1986, p. 1-5, vol. 304, no. 1, pp. 1–5, 1986.
- [27] N. Sartore, E. Ripamonti, A. Treves, and R. Turolla, “Galactic neutron stars i. space and velocity distributions in the disk and in the halo,” *A&A*, vol. 510, no. A23, 02 February 2010.
- [28] X. H. Sun and J. L. Han, “Pulsar motions in our galaxy,” *Monthly Notices of the Royal Astronomical Society*, vol. 350, pp. 232–242, 05 2004.
- [29] D. A. Green, “Some statistics of galactic snrs,” 2005.

## Acknowledgments

I would like to thank the IGR group at the University of Glasgow for supplying both their expertise and knowledge on the nature of Gravitational waves and how LIGO goes on to detect them. I would like to thank Dr. Chris Messenger for supervising this report. His knowledge of both the physics and statistics of the subject were invaluable for the completion of this report.

## Appendix A: Derivation of (18)

For the maximum amplification of the *point mass* lens, we start from Eq.(16) :

$$F(w, y) = e^{\frac{\pi w}{4} + i\frac{w}{2}(\ln(\frac{w}{2}) - 2\phi_m(y))} \Gamma\left(1 - \frac{i}{2}w\right) {}_1F_1\left(\frac{i}{2}w, 1; \frac{i}{2}wy^2\right) \quad (\text{A.1})$$

then using the identity  $|\Gamma(1 + bi)|^2 = \frac{b\pi}{\sinh(b\pi)}$  [13]:

$$|\Gamma(1 - \frac{w}{2}i)|^2 = \frac{\frac{-w}{2}\pi}{\frac{e^{-w\pi/2} - e^{w\pi/2}}{2}} = \frac{w\pi}{1 - e^{-w\pi}} e^{-\frac{-w\pi}{2}} \quad (\text{A.2})$$

inserting this last equation into (16) and taking the modulus of the function:

$$|F(w, y)| = \left| e^{\frac{\pi w}{4}} e^{i\frac{w}{2}(\ln(\frac{w}{2}) - 2\phi_m(y))} \sqrt{\frac{w\pi}{1 - e^{-w\pi}}} e^{-\frac{-w\pi}{4}} {}_1F_1\left(\frac{i}{2}w, 1; \frac{i}{2}wy^2\right) \right| \quad (\text{A.3})$$

then setting  $y = 0$  and using the identity  $\lim_{z \rightarrow 0} {}_1F_1(a, b; z) = 1$  [13], pag.508, Eq.(13.5.5), it follows:

$$|F(w, 0)| = \sqrt{\frac{w\pi}{1 - e^{-w\pi}}} \quad (\text{A.4})$$

the for geometric optics limit, ( $w \gg 1$ ), it reduces to  $|F(w, 0)| = \sqrt{w\pi}$ .

## Appendix B: Derivation of (17) (19)

Starting from equation (13), with  $\psi(x) = x$ , follows:

$$F(w, y) = -iwe^{\frac{i}{2}wy^2} \int_0^\infty x J_0(wxy) e^{iw[\frac{1}{2}x^2 - x + \phi_m(y)]} dx \quad (\text{B.1})$$

Then by expanding the second term in the exponential as an infinite sum, follows:

$$F(w, y) = -iwe^{\frac{i}{2}wy^2 + iw\phi_m(y)} \sum_{n=0}^{\infty} \frac{(-iw)^n}{n!} \int_0^\infty x^{1+n} J_0(wxy) e^{iw([\frac{1}{2}x^2])} dx \quad (\text{B.2})$$

then using the solution found in [13], pag. 505 and the identity  $e^z {}_1F_1(a, b; -x) = {}_1F_1(b - a, b; x)$ , follows:

$$F(w, y) = e^{\frac{i}{2}w(y^2 + 2\phi_m(y))} \sum_{n=0}^{\infty} \frac{\Gamma\left(1 + \frac{n}{2}\right)}{n!} \left(2we^{i3\pi/2}\right)^{n/2} {}_1F_1\left(1 + \frac{n}{2}, 1; -\frac{i}{2}wy^2\right) \quad (\text{B.3})$$

Instead, to solve for the maximum amplification at  $y = 0$  for the SIS model, we start again from (13):

$$\begin{aligned}
F(w, 0) &= -iw \int_0^\infty x e^{iw[\frac{1}{2}x^2 - x]} dx \\
&= -w \int_0^\infty t e^{(w\frac{1}{2}t^2 - i^{1/2}wt)} dt
\end{aligned} \tag{B.4}$$

where the change of variable  $t = \sqrt{i}x$  was inserted in the second part of the equation. Following [12], the equation has a simple form [13], pag. 686:

$$F(w, 0) = e^{\frac{i}{4}w} D_{-2}\left(e^{\frac{i3\pi}{4}} \sqrt{w}\right) \tag{B.5}$$

where  $D_{-2}$  is the parabolic cylinder function, defined as:

$$D_{-2}(z) = \sqrt{\frac{\pi}{2}} e^{\frac{z^2}{4}} \left(1 - \text{Erf}\left(\frac{z}{\sqrt{2}}\right)\right) - e^{\frac{-z^2}{4}} \tag{B.6}$$

Therefore, the maximum amplification factor for the SIS model when  $y = 0$  follows:

$$|F(w, 0)| = \left|1 + \frac{1}{2}(1-i)e^{-\frac{1}{2}w} \sqrt{\pi w} \left[1 + \text{Erf}\left(\frac{\sqrt{w}}{2}(1-i)\right)\right]\right| \tag{B.7}$$